Theoretical Study of the 1,3-Hydrogen Shift of Triazene in Water

I. Fdez. Galván,[†] M. A. Aguilar,*[,†] and M. F. Ruiz-López*[,‡]

Departamento de Química Física, Facultad de Ciencias, Universidad de Extremadura, Avda. de Elvas s/n, 06071 Badajoz, Spain, and Équipe de Chimie et Biochimie Théoriques, UMR CNRS-UHP No. 7565, Université Henri Poincaré−Nancy I, BP 239, 54506 Vandœuvre-lès-Nancy, France

Received: June 1, 2005; In Final Form: October 7, 2005

The 1,3-hydrogen shift of triazene in aqueous solution was studied with a combination of QM/MM methods. First, the different species involved were characterized and the activation free-energies calculated with ASEP/MD, a method that makes use of the mean field approximation. Then the reaction dynamics was simulated with a QM/MM/MD method. A very strong influence of the solvent was observed, both specific, with the participation of a water molecule, and from the rest of the solvent. The effect of solvation on the geometry and electron distribution of triazene is important: N−N bond lengths tend to be more similar and the molecule acquires a planar structure. For the transition state structure, a substantial degree of ionic nature was found. Dynamic solvent effects were also analyzed.

1. Introduction

Triazenes are a class of compounds characterized by the presence of a diazoamino functional group (N═N−N). The simplest member of the family is known just as triazene. These compounds have been used in a variety of applications, ranging from polymer synthesis to anticancer drugs.[1]

A number of studies on the stability, equilibrium, and decomposition of substituted triazenes have been published, both experimental[2−8] and theoretical.[9−13] A general conclusion seems to be that proton transfer between triazenes and solvent is a key initial process for their decomposition and isomerization. Mono- and disubstituted triazenes can exist in two tautomeric forms (RN═N−NHR′ ⇌ RHN−N═NR′), and protonation and deprotonation processes can give rise to cis−trans isomerization and a variety of decomposition products.

Given the interest and versatility of triazenes, and the scarcity, or even absence, of theoretical studies that explicitly include solvent effects, we carried out a theoretical study of the 1,3-proton transfer in *trans*-triazene (HN═N−NH_2 ⇌ H_2N−N═NH), both in vacuo and in aqueous solution. This tautomery is essential for some isomerization processes and can be reasonably expected to be favored by the solvent.

Two mechanisms were considered, represented in Figure 1. The first is a unimolecular process, where one of the protons moves from N3 to N1. The second is a bimolecular process: after the creation of a triazene−water complex, proton interchange occurs between them. For both processes, reactants and transition state structures were optimized in gas phase and in solution, and the free-energy difference between them was evaluated.

Additionally, a study of the dynamical trajectories for the bimolecular reaction in solution was also performed in order to gain further insight into the mechanism and the possible dynamic solvent effects on this reaction. For this part of the study, a combination of QM/MM methods was employed by using the mean field approximation to obtain a representative structure for the transition state, and then, starting from this structure, running a simulation of the course of the reaction.

The rest of the paper is organized as follows. Section 2 describes the computational and theoretical methods used in this work. Section 3 gives additional technical details about the calculations. Section 4 presents the results and a discussion. Finally, Section 5 presents the main conclusions.

2. Method

For the calculation of solvent effects, two methods were used. First, a continuum method was applied, specifically the self-consistent reaction field (SCRF) method developed in Nancy,[14−17] with a cavity shape adapted to the solute and a multicenter multipole expansion for the solute charge distribution.

The second method applied was ASEP/MD (averaged solvent electrostatic potential from molecular dynamics), a QM/MM method that uses the mean field approximation. This method has been described in previous papers.[18,19,20,21] Here, we shall present just a brief outline. For more details and schemes, the reader is referred to said papers.

As mentioned above, ASEP/MD is a method combining QM and MM techniques, with the particularity that QM and MD calculations are alternated. During the MD simulations, the geometry and charge distribution of all molecules is considered as fixed. From the resulting data, the average electrostatic potential generated by the solvent on the solute is obtained. This potential is introduced as a perturbation into the solute's quantum mechanical Hamiltonian, and by solving the associated Schrödinger equation, one gets a new charge distribution for the solute, which is used in the next MD simulation. This iterative process is repeated until the electron distribution of the solute and the solvent structure around it are mutually equilibrated.

The geometries of all species studied were optimized, both in gas phase and in solution, with SCRF and ASEP/MD. In the latter case, we used a technique described in previous work[22,23]

* Corresponding authors. E-mail: maguilar@unex.es (M.A.A.); manuel.ruiz@cbt.uhp-nancy.fr (M.F.R.L.).
† Universidad de Extremadura.
‡ Université Henri Poincaré−Nancy I.

10.1021/jp052900d CCC: $30.25
Published on Web 11/08/2005

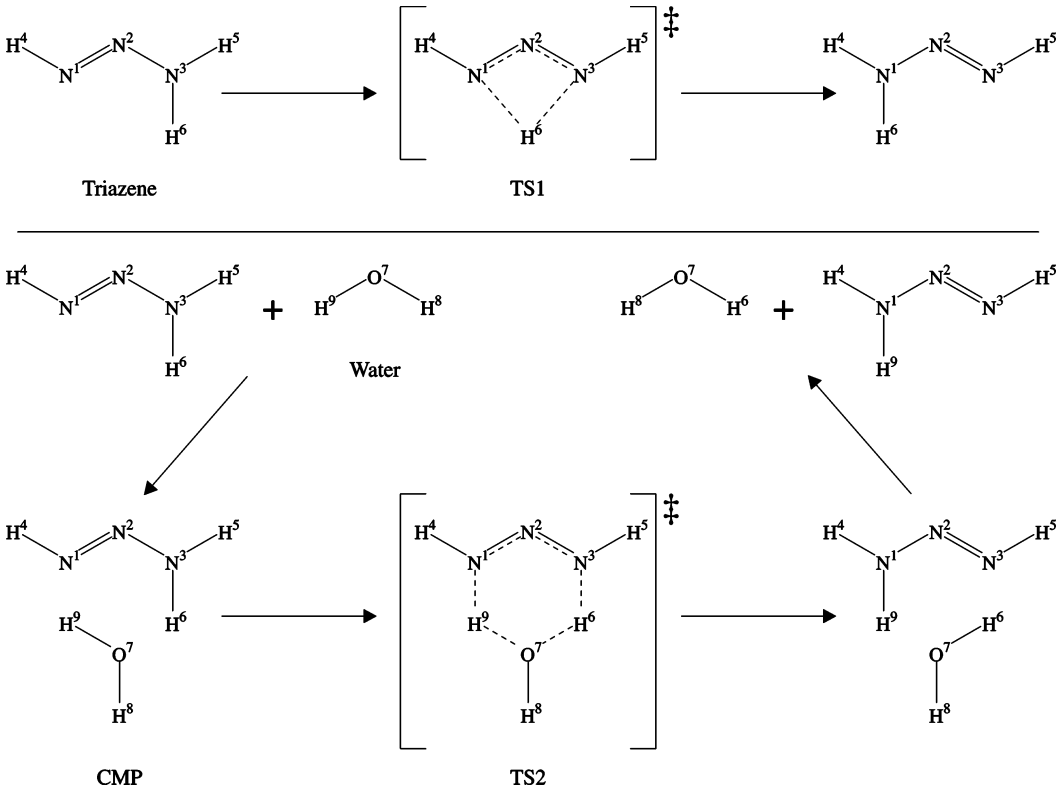

Figure 1. Two studied processes. Above: unimolecular proton shift. Below: bimolecular proton exchange with the formation of an intermediate hydrogen-bonded complex (CMP). Note that both processes are symmetric

based on the combination of ASEP/MD and the free-energy gradient method. At each step of the ASEP/MD procedure, the gradient and Hessian on the system's free-energy surface can be obtained, and so they can be used to search for stationary points on this surface by some optimization method. After each MD simulation, the solute geometry is optimized within the fixed "average" solvent structure by using the free-energy derivatives. In the next MD simulation, the new solute geometry and charge distribution are used. This approach allows the optimization of stable structures as well as transition structures.

The calculation of the free-energy differences was based on an expression of the form of eq 1. In this equation, E_{QM} is the internal quantum mechanical energy of the solute, $\Delta G_{QM/MM}$ is the contribution to the free-energy difference from the solute−solvent interaction and is evaluated classically with the free-energy perturbation (FEP) method,[24−26] and V is the solute's vibrational and thermal contribution to the free-energy and is evaluated with the harmonic approximation. Note that, technically, because the simulations are performed at constant volume, we calculated the Helmholtz free-energy $\Delta A_{QM/MM}$ instead of the Gibbs free energy $\Delta G_{QM/MM}$; however, given the low compressibility of aqueous solutions, these two quantities can be safely equated in this system. This procedure has been satisfactorily applied in previous ASEP/MD studies.[23,27,28]

$$\Delta G = \Delta E_{QM} + \Delta G_{QM/MM} + \Delta V \qquad (1)$$

The reaction dynamics for the bimolecular process was studied by using the "rare event" approach. For reactions with an activation energy significantly larger than thermal fluctuations (around kT), the probability of finding a reactive event in a direct simulation is extremely low, and the process is impractical. The rare event approach[29−31] starts the simulations from the transition state structure and lets the system evolve backward and forward in time. This is a way to consider only the events that eventually reach the transition state.

Reaction trajectories were simulated with the DFMM method developed in Nancy.[32−35] This is a QM/MM method that does not make use of the mean field approximation, but performs a quantum mechanical calculation for each step of a molecular dynamics simulation in which the solute molecule is treated at the quantum level, while solvent molecules are represented with molecular mechanics potentials. This approach allows the study of the solvent effects on the internal dynamics of the solute molecule as well as its electronic structure. In particular, it provides a way to examine the relaxation of the solute structure from the transition state to products (or reactants if run backward). The method has previously been applied to this kind of study,[36,37] and good agreement has been found between ASEP/MD and DFMM results when comparable.[22,38] Here, we show a possible combination of the two methods.

3. Computational Details

Quantum mechanical calculations for the ASEP/MD method were performed with the Gaussian 98 [39] package, while the SCRF method was applied with a modified version[40] of Gaussian 03.[41] For the DFMM quantum mechanical calculations, deMon[42,43] was used. Except when otherwise noted, all calculations were made using DFT with the BP86 functional[44,45] and a basis set of triple-ζ quality (contraction 7111/411/1 for NCO and 411/1 for H) optimized for use with the deMon program (we will call this basis set B1). This level of calculation was chosen because it allows the easiest exchange between the ASEP/MD and DFMM programs. Atomic charges for the solute were calculated with the CHELPG method.[46] Stable structures and transition structures were optimized with the RFO and P-RFO methods,[47−49] respectively.

The SCRF method was applied, as mentioned above, with a multicenter multipole expansion (up to $l = 4$) for the solute and a cavity adapted to the solute's shape. Two cavity sizes were used, one in which Bondi atomic radii[50] were multiplied

by a factor $f = 1.30$ (the default size) and the other with $f = 0.98$ (similar to the PCM default size). A dielectric constant of 78.39 was used in all cases.

For the molecular dynamics simulations, 215 TIP3P water molecules[51] were included in addition to the solute; OPLS[52,53] Lennard−Jones parameters were used for triazene. The simulations were done for a cubic cell of 18.7 Å side length with periodic boundary conditions. A time-step of 0.5 fs was used and the temperature set at 298 K with a Nosé−Hoover thermostat.[54,55] Intermolecular interactions were truncated at 9 Å and long-range electrostatic interactions were evaluated with the Ewald method.[56] Moldy[57] was used for the simulations, which were run for 25 ps of equilibration and 50 ps of production.

The FEP calculations were done with a total of 19 intermediate states for the solute, i.e., an increment in λ, the perturbation parameter, of 0.05. These intermediate states were defined by simple linear interpolation of geometries, atomic charges, and Lennard−Jones parameters between initial and final states. When one of the states corresponded to the separated reactants, they were placed 6 Å apart and a value of 0.025 for $\Delta\lambda$ was used instead (39 intermediate states).

For the simulation of the reaction trajectories in solution, the DFMM program was used. To improve the convergence of the integrations, all hydrogen nuclei in the solute were replaced by deuterium nuclei. The starting configurations for the trajectories were picked from a 500 ps classical MD simulation, keeping the solute rigid in the ASEP/MD optimized TS2 geometry; a total of 50 trajectories were simulated. For each of these trajectories, 0.5 ps were run both forward and backward in time, with a time step of 0.2 fs; by joining these two branches, the complete trajectory was obtained.

The set of initial configurations chosen are a good sample for the solvent distribution around the solute and for the initial velocities of solvent molecules, but because they were picked from a simulation with rigid solute, all the solute internal degrees of freedom have zero initial velocity. To generate a more realistic sample of these velocities, random values were picked in the following way:

(1) The Hessian matrix calculated in solution with ASEP/MD was diagonalized, and the vibrational modes and frequencies were obtained; translational and rotational modes were discarded, and the transition mode was identified (characterized by a negative force constant).

(2) The transition mode was assigned a random kinetic energy in each initial configuration, following a Maxwell−Boltzmann distribution: the probability of having a given energy E is proportional to $\exp(-E/kT)$. The direction for the corresponding velocity was constant in all configurations.

(3) Each of the vibrational modes was assigned a kinetic energy $E_i = (1/4)h\nu_i$, with ν_i being the harmonic frequency of that mode. This energy corresponds to the average kinetic energy of a harmonic oscillator of the same frequency. The direction (sign) of each vibration was chosen randomly.

This last point merits a few extra comments. On one hand, one should note that the kinetic energy of a harmonic oscillator at its equilibrium geometry is $^1/_2h\nu$ (classical limit). On the other hand, the optimized transition state in solution represents a stationary point (actually a saddle point of first order) with respect to a thermodynamic average over solvent configurations. However, for a specific solvent configuration, such a TS geometry does not correspond to a rigorous saddle point, but to some thermal fluctuation around it. Accordingly, the kinetic energy associated with vibrational modes (other than the reaction coordinate) should lie below $^1/_2h\nu$, and on average, one may consider that this kinetic energy will be close to the mean kinetic energy of a harmonic oscillator over a whole period, $^1/_4h\nu$.

TABLE 1: Some Geometric and Electrostatic Parameters for the Triazene Molecule Optimized in Vacuo and in Solution with Two Methods (and Two Cavity Sizes for SCRF)[a]

		SCRF		
	in vacuo	$f = 1.30$	$f = 0.98$	ASEP/MD
N1═N2	1.271	1.275	1.279	1.287
N2−N3	1.354	1.345	1.331	1.322
N3−H5	1.016	1.017	1.018	1.020
N3−H6	1.028	1.027	1.027	1.031
N1═N2−N3−H5	159.0	160.8	163.3	179.3
N1═N2−N3−H6	16.2	16.1	14.4	0.6
q(N1)	−0.398	−0.469	−0.613	−0.636
q(N3)	−0.387	−0.384	−0.331	−0.128
μ	1.70	2.25	2.98	2.96

[a] Distances in Å, angles in deg, charges in e, and dipole moments in D.

TABLE 2: Some Geometric and Electrostatic Parameters for the Triazene−Water Complex (CMP) Optimized in Vacuo and in Solution with Two Methods (and Two Cavity Sizes for SCRF)[a]

		SCRF		
	in vacuo	$f = 1.30$	$f = 0.98$	ASEP/MD
N1−H4	1.031	1.030	1.030	1.033
N3−H5	1.013	1.015	1.016	1.023
N1···H9	1.855	1.805	1.768	1.713
O7···H6	1.962	2.077	3.425	3.102
O7−H8	0.974	0.975	0.976	0.989
N1═N2−N3−H6	7.7	10.2	9.9	0.8
q(O7)	−0.682	−0.800	−0.965	−0.958
q(H8)	0.355	0.425	0.490	0.479

[a] Distances in Å, angles in deg, and charges in e.

4. Results and Discussion

In this section, we present the results obtained for the geometries and free-energy differences of the species studied, both in gas phase and in aqueous solution. Finally, the reaction dynamics results are also discussed.

4.1. Gas Phase. The geometries of all five species shown in Figure 1 were optimized in vacuo by using the default options in Gaussian. The number of negative force constants in the Hessian matrix confirmed the nature of stable structures or transition states in each case. The optimized symmetries agree with those reported by Pye et al.[13] Some of the most important geometric parameters are given in Tables 1−4. Note that values for distances and angles are given within 0.001 Å and 0.1° for comparative purposes with related calculations. However, considering the approximations made, the absolute errors in computed geometries are expected to be a little larger.

Zero-point energies and entropy corrections were also calculated for all species, so that the reaction (or activation) free energy for different processes could be obtained. These energy differences are given in Table 5. As can be seen, the direct unimolecular 1,3-hydrogen shift is highly unfavorable in gas phase, with an activation free energy of more than 30 kcal/mol. The bimolecular path, however, seems to be much shallower, giving a total activation barrier (from free reactants to transition state) of around 10 kcal/mol. The formation of the triazene−water complex from free reactants occurs almost without free-energy change; the enthalpy and entropy variations cancel out.

TABLE 3: Some Geometric and Electrostatic Parameters for the Unimolecular Transition State (TS1) Optimized in Vacuo and in Solution with Two Methods (and Two Cavity Sizes for SCRF)[a]

		SCRF		
	in vacuo	$f = 1.30$	$f = 0.98$	ASEP/MD
N1···N2	1.310	1.311	1.311	1.310
N1−H4	1.027	1.027	1.029	1.033
N1···H6	1.365	1.366	1.368	1.369
H4−N1···N2···N3	162.6	161.3	159.1	164.1
q(N1)	−0.258	−0.269	−0.285	−0.285
q(N2)	−0.130	−0.154	−0.200	−0.172
q(H4)	0.260	0.282	0.315	0.306
μ	0.07	0.10	0.23	0.10

[a] Distances in Å, angles in deg, charges in *e*, and dipole moments in D

TABLE 4: Some Geometric and Electrostatic Parameters for the Bimolecular Transition State (TS2) Optimized in Vacuo and in Solution with Two Methods (and Two Cavity Sizes for SCRF)[a]

		SCRF		
	in vacuo	$f = 1.30$	$f = 0.98$	ASEP/MD
N1···N2	1.307	1.305	1.297	1.297
N1−H4	1.021	1.020	1.019	1.027
N1···H9	1.227	1.175	1.101	1.102
O7···H9	1.305	1.385	1.560	1.545
O7−H8	0.975	0.976	0.977	0.985
N2···N1···H9	112.7	113.5	115.7	116.1
q(O7)	−0.772	−0.962	−1.238	−1.255
q(H8)	0.367	0.411	0.446	0.489
q(H9)	0.228	0.267	0.308	0.302
μ	1.94	3.17	5.83	5.15

[a] Distances in Å, angles in deg, charges in *e*, and dipole moments in D.

TABLE 5: In Vacuo Free-Energy Differences for Several Processes (in kcal/mol)[a]

process	ΔG
$N_3H_3 \rightarrow$ TS1	32.03
$N_3H_3 + H_2O \rightarrow$ CMP	0.86
CMP $\rightarrow$ TS2	9.21
$N_3H_3 + H_2O \rightarrow$ TS2[b]	10.07

[a] TS1, TS2 and CMP refer to the structures in Figure 1. [b] The sum of the two previous processes.

TABLE 6: In Vacuo Activation Free Energies, in kcal/mol, for the Two Studied Reactions Calculated at Different Levels[a]

quantum level	$N_3H_3 \rightarrow$ TS1	$N_3H_3 + H_2O \rightarrow$ TS2
BP86/B1	32.03	10.07
BP86/6-31+G*	34.03	11.46
B3LYP/B1	37.62	16.24
MP2/B1//BP86/B1	39.92	17.73
MP2/6-31+G*[13]	41.37	18.36

[a] B1 is the basis set used in this work.

The energy differences reported by Pye et al.[13] for the same processes are between 8 and 9 kcal/mol higher than those found here. To ascertain the source of these discrepancies, we carried out new optimizations and free-energy calculations at different quantum mechanical levels. The results of these tests are given in Table 6. From these results, one can see that the effect of the basis set is small, raising the activation energies by between 1 and 2 kcal/mol; replacing the BP86 functional by the hybrid B3LYP functional[58,59] gives rise to a much greater increase. The possible effect on the optimized geometry is minimal, as an MP2 calculation on the BP86/B1 geometry yields almost the same results as those of Pye et al. It can thus be concluded that the main source for the disagreements in the activation energies is the use of the BP86 functional, and the introduction of a hybrid functional like B3LYP improves the results. However, it is currently not possible to use hybrid functionals with the DFMM program, and it was preferred to keep the same functional in all the calculations, especially because the errors seem to be systematic, and in any case, the catalytic effect of a water molecule was evaluated at between 22 and 23 kcal/mol.

4.2. Aqueous Solution. All five species were also optimized in solution by using the SCRF continuum method and ASEP/MD. In comparison, with the in vacuo structure, the triazene molecule (Table 1) presents a longer double N═N bond and a shorter N−N bond in solution, and the difference is larger with ASEP/MD than with SCRF (in which case, it is larger with a smaller cavity, as expected). N−H bonds are slightly lengthened with ASEP/MD, but undergo negligible change with SCRF. Another key difference is that ASEP/MD, unlike SCRF and the gas-phase calculations, predicts an almost planar structure for triazene in solution.

Changes in the water molecule are not discussed here. The results agree basically with previous similar studies.[22,32] There is little variation in the geometry, but a major increase in the dipole moment.

For the triazene−water complex (called CMP here, Table 2), the main change when going from the gas phase to aqueous solution is the breaking of the O···H6 hydrogen bond and the shortening of the N1···H9 one, which becomes the only link between the two molecules. A slight stretch of the O−H and N−H bonds not involved in the intermolecular interaction is observed with ASEP/MD. Again, this method predicts a planar structure for triazene, while SCRF gives a pyramidal N3 that is even more pronounced than in vacuo. As for the atomic charges, the most important effect is the polarization of the water molecule, especially in the O−H8 bond.

In this case, the smaller SCRF cavity does not give results closer to ASEP/MD. The larger cavity provides reasonably close results, but the O···H6 bond is not so clearly broken; the smaller cavity gives a totally different orientation for the water molecule, with H6 and H8 almost face to face, as can be seen in Figure 2. This result illustrates one of the limitations of continuum methods, i.e., the strong influence of the cavity characteristics (that cannot be defined unambiguously) on the equilibrium properties of the solute, especially when weak bonds are involved, as in the present case.

For the unimolecular transition state, TS1 (Table 3), changes from vacuum to solution are minimal, but still somewhat greater with ASEP/MD, which does not predict a planar molecule in this case. Atomic charges are lower than in the triazene, which suggests a lower stabilization for the transition state and an increase in activation energy.

For the bimolecular transition state, TS (Table 4), larger changes are observed. Most conspicuously, there is a shortening of N···N bonds and of N−H bonds involved in the reaction (by 0.125 Å), as well as a lengthening of all the O−H bonds (by 0.240 Å for these same H atoms). There is an increase of almost 0.5 *e* in the negative atomic charge on the O, and also an increase in the positive charge on the different H atoms. SCRF with the smaller cavity again gives similar results. The overall effect points to the formation of an ion pair between the protonated triazene $N_3H_4^+$ and the hydroxyl anion OH^-. This major charge separation when going to the aqueous solution

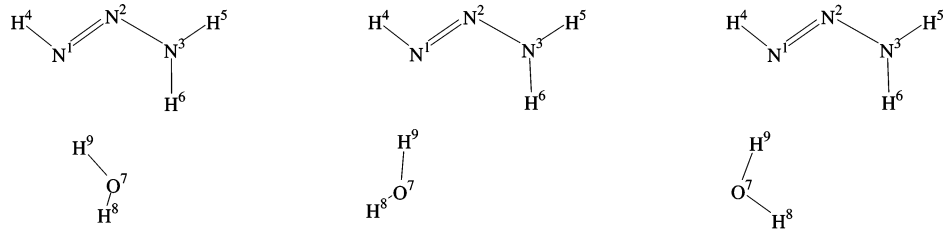

Figure 2. Optimized geometries for the triazene−water complex in vacuo and in solution, with two different methods. H8 is significantly out-of-plane in the two leftmost structures.

TABLE 7: Free-Energy Differences in Solution for Several Processes, in kcal/mol, Calculated with Two Methods (and Two Cavity sizes for SCRF)[a]

	SCRF		ASEP/MD	
process	$f = 1.30$	$f = 0.98$	ΔG	$\Delta G_{QM/MM}$
$N_3H_3 \rightarrow$ TS1	33.93	37.39	34.91	6.13
$N_3H_3 + H_2O \rightarrow$ CMP	4.72	7.95	6.66	0.63
CMP $\rightarrow$ TS2	8.86	11.40	5.46	−8.09

[a] For ASEP/MD, the solute−solvent contribution, $\Delta G_{QM/MM}$, is also shown (see eq 1).

makes it reasonable to assume a decrease of activation energy compared to the gas phase.

Once all the structures were optimized in solution, the corresponding free-energy differences were calculated, and the results are given in Table 7. The unimolecular reaction, with no direct intervention of water molecules, has in all cases a very high activation energy, more than 30 kcal/mol. All the different methods predict an increase in this energy of between 1.9 and 5.4 kcal/mol with respect to the in vacuo value. ASEP/MD provides a reason for this increase: mainly the loss of favorable solute−solvent interactions, reflected in a positive and significant $\Delta^{\ddagger}G_{QM/MM}$ term (6.1 kcal/mol).

The participation of a water molecule clearly favors the proton shift. As previously seen, in gas phase, the activation energy is reduced to around 10 kcal/mol. In solution, the situation is more complicated. Although the free-energy difference between the free reactants and the complex has been calculated, it is not clear what its physical sense is in a case like this, where one of the reactants is the solvent. The usual approach of considering the reactants infinitely apart is not realistic when there is always a solvent molecule, one of the reactants, near the other reactant. Hence, it is not easy to define the "starting point" for a reaction like this one, but it is probably more appropriate to take the energy of the CMP $\rightarrow$ TS2 process as the activation free energy in solution, particularly because, as noted above, the optimized complex in solution is more similar to the reactants, with a single hydrogen bond.

Accepting this as a valid approximation, the activation free energy for the solvent-assisted proton shift according to the ASEP/MD method is 5.46 kcal/mol, almost $^1/_2$ of the in vacuo activation energy. The SCRF results are, as was seen above, dependent on the cavity size. The variation with respect to the gas phase is smaller, and even the sign is not clear; relative to the in vacuo value, the larger cavity gives a lower activation energy, while the smaller cavity gives a higher activation energy. Most of the decrease in activation energy observed with ASEP/MD is due the $\Delta^{\ddagger}G_{QM/MM}$ term, which in this case is negative. This is consistent with the high degree of charge separation found for TS2, making the interaction with the rest of the solvent more favorable for the transition state than for the complex.

As noted above, the theoretical calculation could be underestimated by roughly 8 kcal/mol due to the use of the BP86 density functional. In other words, one may expect an activation free-energy barrier of about 13 kcal/mol. There is at least one experimental measurement of proton shift rate constants in triazenes. Smith et al.[8] determined, from the widening in NMR signals, the tautomerization constants for a series of alkyltriazenes in methanol at 295 K, obtaining values of from 8.5 s^{-1} for 1-methyl-3-*tert*-butyltriazene to 2040 s^{-1} for 1-methyl-3-ethyltriazene. These rate constants correspond to activation energies ranging between 16.0 and 12.8 kcal/mol, according to transition state theory. Obviously, these values cannot be directly compared to that obtained theoretically because they were determined for different systems (alkyltriazenes in methanol instead of triazene in water). Besides, other processes, not considered in the calculations, could play a role in the experimental measurements. Nevertheless, the order of magnitude of the estimated activation energy is correct.

4.3. Reaction Trajectories. A dynamical study was carried out for the bimolecular reaction in solution with the DFMM method and the conditions detailed above. A total of 50 trajectories were simulated, all of them starting with the same solute structure (TS2 optimized with ASEP/MD), but with different solvent distribution and initial velocities. The initial velocities in the transition mode are always directed toward the product state, which was arbitrarily defined as the one where H6 belongs to the water molecule. Of these 50 trajectories, 31 (62%) were found to be reactive (there was a proton exchange) and 19 (38%) nonreactive. Nonreactive trajectories included 11 reactants $\rightarrow$ reactants and 8 products $\rightarrow$ products. We identified a correlation between the initial kinetic energy in the transition mode and the trajectory type. Thus, the average initial kinetic energy for reactive trajectories is 0.76 kcal/mol, whereas for nonreactive trajectories, it is 0.27 kcal/mol. This is an average result, but one should keep in mind that some reactive trajectories have a small initial energy, and similarly, some nonreactive trajectories have large energy values. Nonetheless, of the 12 trajectories with energy higher than 1.0 kcal/mol, 10 were reactive.

With these data, the classical transmission coefficient κ (disregarding the tunneling effect) can be evaluated through eq 2,[60,61] where v_i is the initial velocity in the transition mode of each trajectory, and δ_i is a factor equal to 1 for reactive trajectories and equal to 0 for nonreactive ones.

$$\kappa = \frac{\sum v_i \delta_i}{\sum v_i} \tag{2}$$

In this way, a value of 0.73 is obtained for κ that indicates the existence of significant dynamical effects.

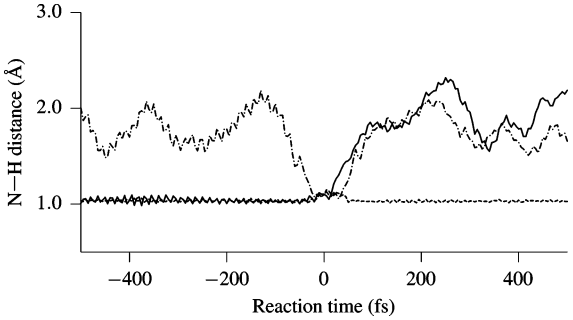

Figure 3. Evolution of the N3−H6 distance in three kinds of trajectories: (—) reactants → products; (- - -) reactants → reactants; (— · —) products → products.

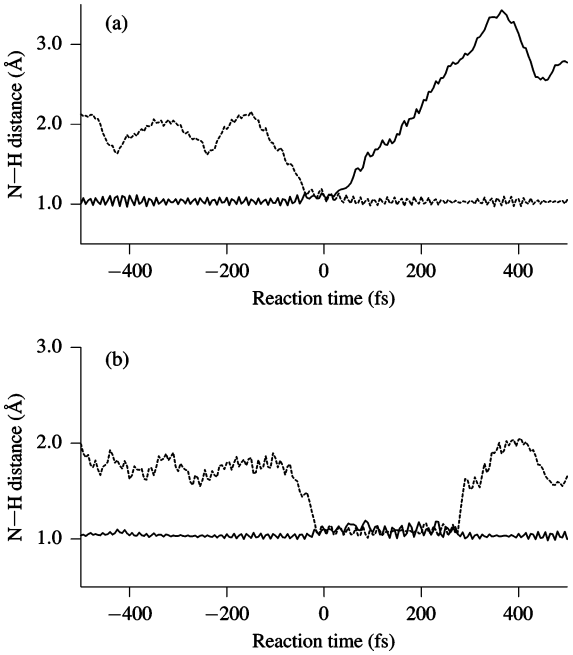

Figure 4. Example trajectories: (—) N3−H6 distance; (- - -) N1−H9 distance.

Figure 3 shows examples of the three different kinds of trajectories computed. The evolution of the N3−H6 distance with time is represented. Time $t = 0$ corresponds to the initial configuration (TS2 structure), so that each trajectory extends to negative and positive times. In the reactive trajectory, the N3−H6 distance increases from 1.0 Å on the reactant side (negative time) up to a typical H-bond distance on the product side (positive time). The bond length begins to increase slightly before reaching the TS (35 fs) and continues to increase after crossing it to reach a maximum value of around 2.3 Å at about 250 fs. For nonreactive trajectories (either reactants → reactants or products → products), one may remark that the N3−H6 distance remains close to its value in the TS roughly from $t = -30$ fs to $t = +30$ fs.

Because the simulated trajectories are started at the transition structure, it is interesting to look at the fate of the ancillary water molecule in reaching the reactant and product regions. In particular, one might ask whether it remains hydrogen-bonded to triazene or moves rapidly into the bulk. The example displayed in Figure 4a illustrates a trajectory in which the water molecule forms a hydrogen bond on the reactant side but not on the product side. Considering the total number of 100 semitrajectories computed in our study and looking at the values of the N−H distances at $t = +0.5$ ps and $t = -0.5$ ps, one finds that only 13 semitrajectories show a clear separation

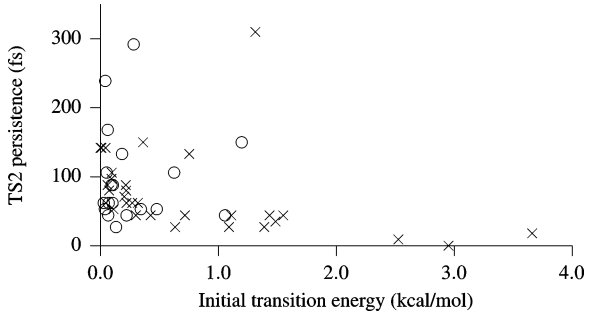

Figure 5. Approximate persistence time of the transition structure versus the initial energy in the transition mode. (×): reactive trajectories. (○): nonreactive trajectories.

between triazene and water. These results confirm that the hydrogen bond between triazene and water is rather stable and support the idea of taking the triazene−water complex as the reference state for free-energy calculations in solution.

Another striking feature in the simulated trajectories is the existence, in many cases, of a significant time interval during which the chemical system's structure resembles that of the transition state. This can be observed in Figure 4b. As shown, the curve corresponds to a nonreactive trajectory in which the N1−H9 and N3−H6 distances oscillate around 1.1 Å for almost 300 fs. Most trajectories exhibit this kind of behavior, although the corresponding time interval may vary substantially. The average length of the interval is around 85 fs, corresponding to 5−6 N−H bond vibrational periods. Note that there are a few trajectories displaying an almost instantaneous process for which this interval is negligible. In Figure 5, we plot the length of this interval versus the kinetic energy assigned to the transition mode for the trajectory. There is no clear relationship between the two quantities, but the analysis of the results shows two main trends: (1) trajectories with a higher energy present smaller persistence intervals, and (2) trajectories with a short persistence interval are often reactive.

The magnitude of the average transition structure lifetime is another manifestation of nonequilibrium solvent effects on the reaction course. The chemical system may be "trapped" at the transition structure so that some solvent reorganization may be required for the system to evolve toward reactants or products. When this occurs, the initial solvated solute structure can be depicted as a metastable state rather than as a saddle point structure. In fact, from the 50 initial configurations considered, only 22 show a negative force constant for the solute (calculated at the QM/MM level). However, although the average TS lifetime is smaller for those trajectories having an initial negative force constant (65 fs vs 99.5 fs for trajectories having positive force constants only), no clear correlation was found between these two properties. A more detailed analysis would need to take into account not only the sign of the initial force constants, but also the velocities of the atoms in the system.

5. Conclusions

In this work we have studied a reaction in solution with the combination of two QM/MM methods, ASEP/MD and DFMM, which were shown to be quite complementary. With ASEP/MD, average structural and thermodynamic properties can easily be obtained, while DFMM allows a detailed examination of the dynamical behavior of the system. Moreover, the transfer of results between these methods is straightforward given their technical similarity.

Regarding the particular system studied, some conclusions can be drawn. First, it is clear that the participation of a water

molecule in the proton-shifting process significantly decreases the activation energy and the overall effect of the solvent is somewhat lower, but still important. Second, in aqueous solution, a structure with a strong charge separation is favored in the transition state, which points to a possible preference for a stepwise mechanism instead of the more concerted mechanism of the present study. Third, the calculated value for the transmission coefficient κ (about 0.7), together with the persistence of the transition structure in many cases, indicates the importance of dynamical solvent effects in this reaction.

Finally, it should be noted that, to make the present study more complete, further investigation of other possible mechanisms (especially protonation and deprotonation) and a better treatment of other factors such as tunneling would be needed. However, in this work, we have described a valid way to combine these two different methods for the study of chemical reactions in solution, which was our primary goal.

Acknowledgment. This research was sponsored by the Consejería de Educación, Ciencia, y Tecnología of the Junta de Extremadura (project 2PR03A071) and the Dirección General de Investigación of the Spanish Ministerio de Educación y Ciencia (project CTQ2004-05680/BQU). I.F.G. thanks the Dirección General de Universidades for supporting his stay at Nancy.

References and Notes

(1) Kimball, D. B.; Haley, M. M. *Angew. Chem., Int. Ed.* **2002**, *41*, 3338.
(2) Scaiano, J. C.; Chen, C.; McGarry, P. F. *J. Photochem. Photobiol., A*: **1991**, *62*, 75.
(3) Barra, M.; Chen, N. *J. Org. Chem.* **2000**, *65*, 5739.
(4) Chen, N.; Barra, M.; Lee, I.; Chahal, N. *J. Org. Chem.* **2002**, *67*, 2271.
(5) Sutherland, J. W. *J. Phys. Chem.* **1979**, *83*, 789.
(6) Smith, R. H., Jr.; Denlinger, C. L.; Kupper, R.; Koepke, S. R.; Michejda, C. J. *J. Am. Chem. Soc.* **1984**, *106*, 1056.
(7) Smith, R. H., Jr.; Denlinger, C. L.; Kupper, R.; Mehl, A. F.; Michejda, C. J. *J. Am. Chem. Soc.* **1986**, *108*, 3726.
(8) Smith, R. H., Jr.; Wladkowski, B. D.; Mehl, A. F.; Cleveland, M. J.; Rudrow, E. A.; Chmurny, G. N.; Michejda, C. J. *J. Org. Chem.* **1989**, *54*, 1036.
(9) Ramos, M. N.; Pereira, S. R. *J. Chem. Soc., Perkin Trans.* **1986**, *1986*, 131.
(10) Schmiedekamp, A.; Smith, R. H., Jr.; Michejda, C. J. *J. Org. Chem.* **1988**, *53*, 3433.
(11) Schmiedekamp, A.; Topol, I. A.; Burt, S. K.; Razafinjanahary, H.; Chermette, H.; Pfaltzgraff, T.; Michejda, C. J. *J. Comput. Chem.* **1994**, *15*, 875.
(12) Charbonneau, P.; Jean-Claude, B.; Whitehead, M. A. *J. Mol. Struct. (THEOCHEM)* **2001**, *574*, 85.
(13) Pye, C. C.; Vaughan, K.; Glister, J. F. *Can. J. Chem.* **2002**, *80*, 447.
(14) Rivail, J.-L.; Rinaldi, D. *Chem. Phys.* **1976**, *18*, 233.
(15) Rinaldi, D.; Ruiz-López, M. F.; Rivail, J.-L. *J. Chem. Phys.* **1983**, *78*, 834.
(16) Dillet, V.; Rinaldi, D.; Rivail, J.-L. *J. Phys. Chem.* **1994**, *98*, 5034.
(17) Curutchet, C.; Cramer, C. J.; Truhlar, D. G.; Ruiz-López, M. F.; Rinaldi, D.; Orozco, M.; Luque, F. J. *J. Comput. Chem.* **2003**, *24*, 284.
(18) Sánchez, M. L.; Aguilar, M. A.; Olivares del Valle, F. J. *J. Comput. Chem.* **1997**, *18*, 313.
(19) Sánchez, M. L.; Martín, M. E.; Aguilar, M. A.; Olivares del Valle, F. J. *J. Comput. Chem.* **2000**, *21*, 705.
(20) Sánchez, M. L.; Martín, M. E.; Fdez. Galván, I.; Olivares del Valle, F. J.; Aguilar, M. A. *J. Phys. Chem. B* **2002**, *106*, 4813.
(21) Fdez. Galván, I.; Sánchez, M. L.; Martín, M. E.; Olivares del Valle, F. J.; Aguilar, M. A. *Comput. Phys. Commun.* **2003**, *155*, 244.
(22) Fdez. Galván, I.; Sánchez, M. L.; Martín, M. E.; Olivares del Valle, F. J.; Aguilar, M. A. *J. Chem. Phys.* **2003**, *118*, 255.
(23) Fdez. Galván, I.; Martín, M. E.; Aguilar, M. A. *J. Comput. Chem.* **2004**, *25*, 1227.
(24) Zwanzig, R. W. *J. Chem. Phys.* **1954**, *22*, 1420.
(25) Kollman, P. A. *Chem. Rev.* **1993**, *93*, 2395.
(26) Chipot, C.; Pearlman, D. A. *Mol. Simul.* **2002**, *28*, 1.
(27) Fdez. Galván, I.; Olivares del Valle, F. J.; Martín, M. E.; Aguilar, M. A. *Theor. Chem. Acc.* **2004**, *111*, 196.
(28) Corchado, J. C.; Sánchez, M. L.; Aguilar, M. A. *J. Am. Chem. Soc.* **2004**, *126*, 7311.
(29) Keck, J. *Discuss. Faraday Soc.* **1962**, *33*, 173.
(30) Anderson, J. B. *J. Chem. Phys.* **1973**, *58*, 4684.
(31) Chandler, D. In *Classical and Quantum Dynamics in Condensed Phase Simulations*; Berne, B. J., Ciccotti, G., Coker, D. F., Eds.; World Scientific: River Edge, NJ, 1998; pp 3−23.
(32) Tuñón, I.; Martins-Costa, M. T. C.; Millot, C.; Ruiz-López, M. F. *J. Mol. Model.* **1995**, *1*, 196.
(33) Tuñón, I.; Martins-Costa, M. T. C.; Millot, C.; Ruiz-López, M. F.; Rivail, J.-L. *J. Comput. Chem.* **1996**, *17*, 19.
(34) Tuñón, I.; Martins-Costa, M. T. C.; Millot, C.; Ruiz-López, M. F. *J. Chem. Phys.* **1997**, *106*, 3633.
(35) Chalmet, S.; Ruiz-López, M. F. *J. Chem. Phys.* **1999**, *111*, 1117.
(36) Strnad, M.; Martins-Costa, M. T. C.; Millot, C.; Tuñón, I.; Ruiz-López, M. F.; Rivail, J.-L. *J. Chem. Phys.* **1997**, *106*, 3643.
(37) Chalmet, S.; Harb, W.; Ruiz-López, M. F. *J. Phys. Chem. A* **2001**, *105*, 11574.
(38) Martín, M. E.; Aguilar, M. A.; Chalmet, S.; Ruiz-López, M. F. *Chem. Phys. Lett.* **2001**, *344*, 107.
(39) Frisch, M. J.; Trucks, G. W.; Schlegel, H. B.; Scuseria, G. E.; Robb, M. A.; Cheeseman, J. R.; Zakrzewski, V. G.; Montgomery, J. A., Jr.; Stratmann, R. E.; Burant, J. C.; Dapprich, S.; Millam, J. M.; Daniels, A. D.; Kudin, K. N.; Strain, M. C.; Farkas, O.; Tomasi, J.; Barone, V.; Cossi, M.; Cammi, R.; Mennucci, B.; Pomelli, C.; Adamo, C.; Clifford, S.; Ochterski, J.; Petersson, G. A.; Ayala, P. Y.; Cui, Q.; Morokuma, K.; Malick, D. K.; Rabuck, A. D.; Raghavachari, K.; Foresman, J. B.; Cioslowski, J.; Ortiz, J. V.; Stefanov, B. B.; Liu, G.; Liashenko, A.; Piskorz, P.; Komaromi, I.; Gomperts, R.; Martin, R. L.; Fox, D. J.; Keith, T.; Al-Laham, M. A.; Peng, C. Y.; Nanayakkara, A.; Gonzalez, C.; Challacombe, M.; Gill, P. M. W.; Johnson, B. G.; Chen, W.; Wong, M. W.; Andres, J. L.; Head-Gordon, M.; Replogle, E. S.; Pople, J. A. *Gaussian 98*, revision A.11.3; Gaussian, Inc.: Pittsburgh, PA, 2001.
(40) Rinaldi, D.; Bouchy, A.; Rivail, J.-L.; Dillet, V. *J. Chem. Phys.* **2004**, *120*, 2343.
(41) Frisch, M. J.; Trucks, G. W.; Schlegel, H. B.; Scuseria, G. E.; Robb, M. A.; Cheeseman, J. R.; Montgomery, J. A., Jr.; Vreven, T.; Kudin, K. N.; Burant, J. C.; Millam, J. M.; Iyengar, S. S.; Tomasi, J.; Barone, V.; Mennucci, B.; Cossi, M.; Scalmani, G.; Rega, N.; Petersson, G. A.; Nakatsuji, H.; Hada, M.; Ehara, M.; Toyota, K.; Fukuda, R.; Hasegawa, J.; Ishida, M.; Nakajima, T.; Honda, Y.; Kitao, O.; Nakai, H.; Klene, M.; Li, X.; Knox, J. E.; Hratchian, H. P.; Cross, J. B.; Bakken, V.; Adamo, C.; Jaramillo, J.; Gomperts, R.; Stratmann, R. E.; Yazyev, O.; Austin, A. J.; Cammi, R.; Pomelli, C.; Ochterski, J. W.; Ayala, P. Y.; Morokuma, K.; Voth, G. A.; Salvador, P.; Dannenberg, J. J.; Zakrzewski, V. G.; Dapprich, S.; Daniels, A. D.; Strain, M. C.; Farkas, O.; Malick, D. K.; Rabuck, A. D.; Raghavachari, K.; Foresman, J. B.; Ortiz, J. V.; Cui, Q.; Baboul, A. G.; Clifford, S.; Cioslowski, J.; Stefanov, B. B.; Liu, G.; Liashenko, A.; Piskorz, P.; Komaromi, I.; Martin, R. L.; Fox, D. J.; Keith, T.; Al-Laham, M. A.; Peng, C. Y.; Nanayakkara, A.; Challacombe, M.; Gill, P. M. W.; Johnson, B.; Chen, W.; Wong, M. W.; Gonzalez, C.; Pople, J. A. *Gaussian 03*, revision B.05; Gaussian, Inc.: Wallingford, CT, 2004.
(42) St-Amant, A.; Salahub, D. R. *Chem. Phys. Lett.* **1990**, *169*, 387.
(43) Godbout, N.; Salahub, D. R.; Andzelm, J.; Wimmer, E. *Can. J. Chem.* **1992**, *70*, 560.
(44) Becke, A. D. *Phys. Rev. A* **1988**, *38*, 3098.
(45) Perdew, J. P. *Phys. Rev. B* **1986**, *33*, 8822.
(46) Breneman, C. M.; Wiberg, K. B. *J. Comput. Chem.* **1990**, *11*, 361.
(47) Simons, J.; Jørgensen, P.; Taylor, H.; Ozment, J. *J. Phys. Chem.* **1983**, *87*, 2745.
(48) Banerjee, A.; Adams, N.; Simons, J.; Shepard, R. *J. Phys. Chem.* **1985**, *89*, 52.
(49) Baker, J. *J. Comput. Chem.* **1986**, *7*, 385.
(50) Bondi, A. *J. Phys. Chem.* **1964**, *68*, 441.
(51) Jorgensen, W. L.; Chandrasekhar, J.; Madura, J. D.; Impey, R. W.; Klein, M. L. *J. Chem. Phys.* **1983**, *79*, 926.
(52) Jorgensen, W. L.; Swenson, C. J. *J. Am. Chem. Soc.* **1985**, *107*, 569.
(53) Jorgensen, W. L.; Maxwell, D. S.; Tirado-Rives, J. *J. Am. Chem. Soc.* **1996**, *118*, 11225.
(54) Nosé, S. *Mol. Phys.* **1984**, *52*, 255.
(55) Hoover, W. G. *Phys. Rev. A* **1985**, *31*, 1695.
(56) Ewald, P. P. *Ann. Phys. (Leipzig)* **1921**, *64*, 253.
(57) Refson, K. *Comput. Phys. Commun.* **2000**, *126*, 310.
(58) Lee, C.; Yang, W.; Parr, R. G. *Phys. Rev. B* **1988**, *37*, 785.
(59) Becke, A. D. *J. Chem. Phys.* **1993**, *98*, 5648.
(60) Bergsma, J. P.; Reimers, J. R.; Wilson, K. R.; Hynes, J. T. *J. Chem. Phys.* **1986**, *85*, 5625.
(61) Gertner, B. J.; Wilson, K. R.; Hynes, J. T. *J. Chem. Phys.* **1989**, *90*, 3537.